Acta Crystallographica Section D
Biological Crystallography
ISSN 0907-4449

The structure of the caspase recruitment domain of BinCARD reveals that all three cysteines can be oxidized

Kai-En Chen,[a]‡§ Ayanthi A. Richards,[b,c]‡ Tom T. Caradoc-Davies,[d] Parimala R. Vajjhala,[c] Gautier Robin,[a]¶ Linda H. L. Lua,[d] Justine M. Hill,[c,e] Kate Schroder,[b] Matthew J. Sweet,[b] Stuart Kellie,[b,c,f]* Bostjan Kobe[a,c,f] and Jennifer Martin[a,c]*

[a]Division of Chemistry and Structural Biology, Institute for Molecular Bioscience, University of Queensland, Brisbane, Queensland 4072, Australia, [b]Division of Molecular Genetics and Development, Institute for Molecular Bioscience, University of Queensland, Brisbane, Queensland 4072, Australia, [c]School of Chemistry and Molecular Biosciences, University of Queensland, Brisbane, Queensland 4072, Australia, [d]Australian Synchrotron, 800 Blackburn Road, Clayton, Melbourne, Victoria 3168, Australia, [e]Centre for Advanced Imaging, University of Queensland, Brisbane, Queensland 4072, Australia, and [f]Australian Infectious Diseases Research Centre, The University of Queensland, Brisbane, Queensland 4072, Australia

‡ These authors contributed equally.
§ Present address: Academia Sinica, Taiwan.
¶ Present address: BioXtal, Marseille, France and IRCM, Montpellier, France.

Correspondence e-mail: s.kellie@uq.edu.au, j.martin@imb.uq.edu.au

Received 27 November 2012
Accepted 16 January 2013

PDB References: caspase recruitment domain of BinCARD, native, 4dwn; SeMet-labelled, 4fh0

The caspase recruitment domain (CARD) is present in death-domain superfamily proteins involved in inflammation and apoptosis. BinCARD is named for its ability to interact with Bcl10 and inhibit downstream signalling. Human BinCARD is expressed as two isoforms that encode the same N-terminal CARD region but which differ considerably in their C-termini. Both isoforms are expressed in immune cells, although BinCARD-2 is much more highly expressed. Crystals of the CARD fold common to both had low symmetry (space group *P*1). Molecular replacement was unsuccessful in this low-symmetry space group and, as the construct contains no methionines, first one and then two residues were engineered to methionine for MAD phasing. The double-methionine variant was produced as a selenomethionine derivative, which was crystallized and the structure was solved using data measured at two wavelengths. The crystal structures of the native and selenomethionine double mutant were refined to high resolution (1.58 and 1.40 Å resolution, respectively), revealing the presence of a *cis*-peptide bond between Tyr39 and Pro40. Unexpectedly, the native crystal structure revealed that all three cysteines were oxidized. The mitochondrial localization of BinCARD-2 and the susceptibility of its CARD region to redox modification points to the intriguing possibility of a redox-regulatory role.

1. Introduction

Proteins containing a caspase recruitment domain (CARD) are members of the death-domain superfamily that share a six-α-helix bundle topology. This superfamily includes members of the death-domain, the death-effector domain and the pyrin-domain families, each of which has important regulatory roles in the immune response and apoptosis (Kersse *et al.*, 2011).

Bcl10-interacting CARD (BinCARD) is a predicted CARD protein. According to the UniProt knowledgebase (http://www.uniprot.org) the mouse genome encodes one BinCARD isoform, whereas the human gene (*C9orf89*) generates two alternative splice isoforms: BinCARD-1 and BinCARD-2. BinCARD-1 is likely to be a consequence of intron retention (Fig. 1*a*). Both isoforms are identical in sequence up to residue 101, which includes the CARD fold, but bear no resemblance to each other thereafter (Fig. 1*b*).

BinCARD-1 has an additional 127 C-terminal residues and has been reported to bind to Bcl10, a cytoplasmic CARD protein that regulates the function of immune cells including macrophages, T cells and B cells (Thome & Tschopp, 2002). A major role of Bcl10 is the activation of the nuclear factor-κB

(NF-κB) transcription factor through CARD–CARD interactions (Ruland *et al.*, 2001). Unusually, the interaction of BinCARD-1 with Bcl-10 inhibits the NF-κB pathway (Woo *et al.*, 2004). BinCARD-2 is the REFSEQ form (Pruitt *et al.*, 2009) and has an additional 82 C-terminal residues after the CARD, including a predicted 20-residue transmembrane domain.

We are interested in the structure and function of proteins that play a role in immunity (Puri *et al.*, 2006). Microarray experiments suggested that BinCARD mRNA was highly expressed in mouse macrophages. To confirm the relative levels of expression of the two human BinCARD splice isoforms in immune cells, we performed real-time quantitative polymerase chain reaction analysis of mononuclear and polymorphonuclear immune-cell subsets. These data showed that both human BinCARD isoforms are widely expressed among these cells, but were most highly expressed in myeloid cells (polymorphonuclear granulocytes, $CD14^+$ monocytes, monocyte-derived macrophages and dendritic cells) in comparison to $CD3^+$ T cells, $CD19^+$ B cells and $CD56^+$ NK/NKT cells (Supplementary Fig. S1A[1]). In all peripheral blood cell fractions BinCARD-2 appears to be the dominantly expressed isoform. We therefore set out to characterize the structure of human BinCARD.

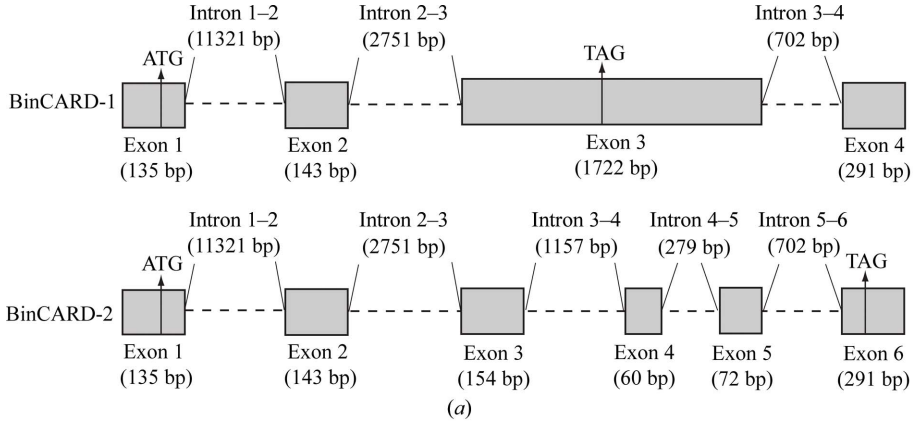

(*a*)

```
BinCARD-1     1 MTDQTYCDRLVQDTPFLTGHGRLSEQQVDRIILQLNRYYPQILTNKEAEKFRNPKASLRV 60
BinCARD-2     1 MTDQTYCDRLVQDTPFLTGHGRLSEQQVDRIILQLNRYYPQILTNKEAEKFRNPKASLRV 60

BinCARD-1    61 RLCDLLSHLQRSGERDCQEFYRALYIHAQPLHSRLPSRHALRKFHITNHACLVLARGGHP 120
BinCARD-2    61 RLCDLLSHLQRSGERDCQEFYRALYIHAQPLHSRLPSRHALQ-----NSDCTELDSGSQS 115

BinCARD-1   121 SLPLMAWMSSMTTQVCCSPGLASPLASAPPQRPPSGPEGRVWQAQAVQMLVSVSHFLPLP 180
BinCARD-2   116 GELSNRGPMSFLAGLGLAVGLALLLYCYPPD-----PKG----------LPGTRRVLGFS 160

BinCARD-1   181 PSLSHGSFHTAWGILYVHSCPSFSNLIPRGSLHVCVDSNLVPTAAWRS 228
BinCARD-2   161 PVIIDR--HVSR-YLLAFLADDLGGL---------------------- 183
```

(*b*)

Figure 1
Splice variants of human BinCARD. (*a*) The two human BinCARD isoforms share identical exons 1–3. The longer isoform, BinCARD-1, is a consequence of the extension of exon 3. The shorter isoform, BinCARD-2, consists of six short exon sequences. The genomic sequence information is from the Ensembl genome database. (*b*) Sequence alignment of the two human BinCARD protein isoforms. Residue numbers correspond to the full-length proteins. Conserved residues are shown in red and the predicted transmembrane helix of BinCARD-2 is highlighted in grey. Residues 1–101 are the same for the two isoforms. This sequence alignment was generated using *ClustalW* from Network Protein Sequence Analysis using default parameters (Combet *et al.*, 2000).

2. Materials and methods

2.1. Summary of BinCARD constructs used

BinCARD-1 (full-length human BinCARD isoform 1), BinCARD-2 (full-length human BinCARD isoform 2), BinCARD-N (residues 1–100 common to both isoforms) and BinCARD-CARD (residues 3–101 common to both isoforms) were used to generate crystals; BinCARD-2-Δ124–183 (residues 2–123 of isoform 2) gave a soluble form of the protein for *in vitro* studies of oligomeric state.

2.2. Oligomeric state

Multi-angle laser light scattering (MALLS) was performed by injecting 100 µl BinCARD-2-Δ124–183 at 5 mg ml^{-1} onto a Superdex 75 10/300 GL column (GE Healthcare) equilibrated with 25 m*M* HEPES pH 7.5, 150 m*M* NaCl, 2 m*M* DTT. The molecular weight was measured using a DAWN HELEOS II laser-light detector connected to an Optilab refractive-index detector (Wyatt Technology). All calculations were performed with the *ASTRA* software (Wyatt Technology).

2.3. Recombinant protein production

BinCARD-CARD (residues 3–101) and BinCARD-2-Δ124–183 (residues 2–123 of BinCARD isoform 2) were amplified from a gene encoding full-length human BinCARD-2 (Open Biosystems). The amplified gene product was ligated into the N-terminal His-tag pMCSG7 vector using ligation-independent cloning (Stols *et al.*, 2002). This vector was transformed into *Escherichia coli* BL21(DE3)pLysS cells and expressed at 298 K for 24 h by autoinduction (Studier, 2005).

A cell pellet from a 1 l culture was lysed in 150 ml 50 m*M* HEPES pH 7.5, 300 m*M* NaCl, 5 m*M* $MgCl_2$, 1% Triton X-100, 25 µg ml^{-1} DNase (Sigma–Aldrich), 100 µl protease-inhibitor cocktail III (AG Scientific Inc.). Supernatant from the cell lysate was incubated with 5 ml TALON cobalt resin (Clontech) for 2 h with rotation. The resin was washed with 100 ml wash buffer consisting of 50 m*M* HEPES pH 7.5, 300 m*M* NaCl, 20 m*M* imidazole. The His-tagged CARD of BinCARD was eluted from the resin with elution buffer consisting of 50 m*M* HEPES pH 7.5, 300 m*M* NaCl, 300 m*M* imidazole.

The His tag was removed by adding 1 mg tobacco etch virus (TEV) protease per 100 mg of eluted protein. The mixture was dialysed for 48 h in 3500 Da molecular-weight cutoff

[1] Supplementary material has been deposited in the IUCr electronic archive (Reference: TZ5022). Services for accessing this material are described at the back of the journal.

membrane tubing (Pacific Lab) against 2 l 50 m*M* HEPES, 300 m*M* NaCl, 2 m*M* fresh DTT at 277 K. After dialysis, cleaved and uncleaved proteins were separated using TALON cobalt metal-affinity resin (Clontech). The flowthrough containing the His-tag-cleaved protein was collected and was further purified by size-exclusion chromatography (SEC) on a Superdex 75 16/60 column (GE Healthcare) equilibrated with SEC buffer consisting of 25 m*M* HEPES pH 7.5, 150 m*M* NaCl, 2 m*M* fresh DTT.

The F16M/L66M double mutant of BinCARD-CARD was engineered for crystal structure phasing purposes and was produced using the QuikChange site-directed mutagenesis protocol (Stratagene). Seleno-DL-methionine (SeMet) labelled BinCARD-CARD double mutant was produced using a previously described method (Edeling *et al.*, 2001) by transforming the variant into *E. coli* BL21(DE3) cells and expressing it in minimal medium containing 100 µg SeMet per litre of culture at 298 K with IPTG induction. Purification of the SeMet-BinCARD double mutant followed the same procedure as used for the native protein.

2.4. Crystallization and data collection

Crystals of native BinCARD-CARD grew in two different conditions from hanging-drop vapour-diffusion experiments performed at room temperature using 32 mg ml^{-1} protein. The first condition consisted of 50 m*M* HEPES pH 7.0, 100 m*M* ammonium sulfate, 5% DMSO, 15% PEG 8000 and 1 m*M* each of reduced and oxidized L-glutathione. The second condition consisted of 100 m*M* bis-tris pH 6.5, 200 m*M* ammonium sulfate, 25% PEG 3350. The best crystals of native BinCARD-CARD were obtained by streak-seeding crystals grown in the first condition at 32 mg ml^{-1} protein into the same condition prepared with protein at 8 mg ml^{-1}. For SeMet-BinCARD, the best crystals were obtained using the second condition with streak-seeding. Prior to data collection, both native and SeMet-labelled crystals were soaked in well solutions augmented with cryoprotectants consisting of 15% and 10% PEG 400, respectively. The crystals were then flash-cooled in liquid nitrogen.

X-ray diffraction data were measured on the MX2 beamline at the Australian Synchrotron at 100 K using the *Blu-Ice* software (McPhillips *et al.*, 2002). The presence of a selenium signal in the SeMet crystal was confirmed by a fluorescence excitation scan at a wavelength of 0.9537 Å. A total of 1080° of diffraction data were measured at each of two wavelengths (remote, 0.9537 Å; inflection, 0.9797 Å). Data were indexed and integrated by *XDS* (Kabsch, 2010) and scaled using *SCALA* (Winn *et al.*, 2011).

2.5. Structure determination

Heavy-atom position determination and initial model building were carried out by *SHELXC*/*D*/*E* (Sheldrick, 2010) and *autoSHARP* (Vonrhein *et al.*, 2007). Structure refinement was performed using *PHENIX* (Adams *et al.*, 2010). The *B*-factor model used for both the native and SeMet mutant structures was isotropic. H atoms (riding model) and water molecules were added automatically during refinement in *PHENIX*. Several rounds of refinement were performed with manual rebuilding in *Coot* (Emsley & Cowtan, 2004), followed by further refinement in *PHENIX*. The quality and geometry of the refined structures were evaluated by *MolProbity* (Chen *et al.*, 2010). Residue Cys63 was modelled as a cysteine sulfenic acid (CSO) in the two molecules in the asymmetric unit. The electron density for CSO63 also suggested an alternative conformation. The final model of the native structure contained 96 residues and 153 water molecules. Residues Ser3, Asn2 and Ala1 at the N-terminus and Ala100 and Leu101 at the C-terminus were disordered, and were not included in the final model. Structure figures were produced using *PyMOL* and structure comparisons were performed using *DALI* (Holm & Rosenström, 2010). The coordinates and structure factors have been deposited in the Protein Data Bank with PDB codes 4dwn and 4fh0 for the native and SeMet-labelled protein, respectively.

2.6. Antibodies and constructs for mammalian cell expression

The polyclonal anti-HA (H6908) antibody was obtained from Sigma–Aldrich. The anti-V5 monoclonal antibody (MCA1360) was obtained from AbD Serotec and rabbit monoclonal anti-Bcl-x_L (54H6) was obtained from Cell Signalling Technology. Fluorescent secondary antibodies (Alexa 488-conjugated and Alexa 594-conjugated) were obtained from Molecular Probes.

The expression construct for ICMT-GFP (Dai *et al.*, 1998) has been described previously. For mammalian cell expression, human isoforms BinCARD-1 and BinCARD-2 were amplified from human monocyte-derived macrophage cDNA and cloned into pEF6/V5-HisTOPO (Invitrogen) in frame with a C-terminal V5 and His tag. The CARD region of BinCARD (BinCARD-N) consisting of residues 1–100 (identical in BinCARD-1 and BinCARD-2) was amplified using the primers 5′-ACCATGACAGATCAGACCTATTGTGACC-3′ (sense) and 5′-AGCGTGGCGGCTGGGCAGG-3′ (antisense) and similarly cloned into the same expression vector.

2.7. Peripheral blood mononuclear cell fractionation and real-time qPCR

Fresh peripheral blood was fractionated into polymorphonuclear, mononuclear and erythrocyte fractions using a double Histopaque 1119/1077 gradient (Sigma). $CD14^+$ monocytes, $CD4^+$ T cells, $CD19^+$ B cells and $CD56^+$ natural killer (NK) and NKT cells were purified from the mononuclear fraction according to standard protocols (Miltenyi Biotec). Human monocyte-derived dendritic cells (HMDCs) and human monocyte-derived macrophages (HMDMs) were differentiated for 7 d with GM-CSF (100 ng ml^{-1}) plus IL-4 (25 ng ml^{-1}) or M-CSF (100 ng ml^{-1}), respectively (all from Immunotools). The preparations of $CD14^+$ and $CD3^+$ cells were 97–99% pure, while the less abundant cell types were enriched (55% $CD19^+$ B cells, 70% $CD56^+$ NK and NKT cells). Isolation of total RNA from individual cell populations and subsequent cDNA synthesis and analysis by real-time

Table 1
Data-processing, phasing and refinement statistics.

Values in parentheses are for the highest resolution shell.

		SeMet-labelled (F16M, L66M)	
	Native	Remote	Inflection point
Space group	*P*1	*P*1	*P*1
Wavelength (Å)	0.9537	0.9537	0.9797
Resolution (Å)	41.11–1.57 (1.64–1.57)	40.7–1.40 (1.50–1.40)	40.67–1.40 (1.47–1.40)
Unit-cell parameters (Å, °)	a = 32.1, b = 36.5, c = 43.8, α = 71.5, β = 90.3, γ = 68.9	a = 32.2, b = 36.7, c = 43.7, α = 108.5, β = 90.3, γ = 111.0	a = 32.2, b = 36.6, c = 43.3, α = 108.5, β = 90.3, γ = 110.9
Total observations	91718	236909	234284
Unique reflections	23456	32997	32797
Completeness (%)	96.4 (90.6)	96.5 (93.3)	95.8 (92.4)
$R_{\rm merge}$†	0.052 (0.34)	0.06 (0.28)	0.08 (0.58)
$\langle I/\sigma(I)\rangle$	25.8 (3.73)	22.0 (7.5)	16.2 (4.4)
Multiplicity	3.9 (3.6)	7.2 (7.3)	7.1 (7.0)
Phasing statistics			
No. of selenium sites expected/found		4/4	
Overall CC‡		0.691	
Overall FOM‡		0.482	
Refinement statistics			
Resolution (Å)	29.66–1.58 (1.64–1.58)	27.72–1.40 (1.44–1.40)	
$R_{\rm work}/R_{\rm free}$§	0.163/0.199	0.137/0.177	
No. of protein atoms (not including H)	1648	1647	
No. of waters	154	206	
No. of other atoms (sulfate)	3	3	
Wilson B factor (Å^2)	18	12	
Average B factor¶ (Å^2)			
Protein	24.8	17.0	
Water	31.1	28.7	
Sulfate	37.5	27.9	
R.m.s. deviations			
Bond lengths (Å)	0.013	0.010	
Bond angles (°)	1.4	1.3	
Ramachandran plot†† (%)			
Favoured	97.9	98.4	
Outliers	0.0	0.0	

† $R_{\rm merge} = \sum_{hkl}\sum_i |I_i(hkl) - \langle I(hkl)\rangle|/\sum_{hkl}\sum_i I_i(hkl)$, where $I_i(hkl)$ is the ith observation of the intensity of the reflection hkl. ‡ Calculated using *autoSHARP* (Vonrhein *et al.*, 2007). § $R_{\rm work} = \sum_{hkl}||F_{\rm obs}| - |F_{\rm calc}||/\sum_{hkl}|F_{\rm obs}|$, where $F_{\rm obs}$ and $F_{\rm calc}$ are the observed and calculated structure-factor amplitudes for each reflection hkl. $R_{\rm free}$ was calculated with 5% of the diffraction data that were selected randomly and excluded from refinement. ¶ Calculated using *BAVERAGE* (Winn *et al.*, 2011) †† Calculated using *MolProbity* (Chen *et al.*, 2010).

qPCR were performed as described previously (Schroder *et al.*, 2012). Specific primers were used for BinCARD-1 [5′-GCCCGTTGACTAACTATGCTCT-3′ (forward) and 5′-GGCAGCAGGGAGGTGTTAC-3′ (reverse)] and BinCARD-2 [5′-GACTGCCAGGAGTTCTACCG-3′ (forward) and 5′-CATGGGTCCCCTGTTACTCA-3′ (reverse)]. BinCARD expression levels were normalized to the housekeeping gene hypoxanthine guanine phosphoribosyl transferase (HPRT).

2.8. Cell culture and transfection

All cell-culture reagents were obtained from Invitrogen. HeLa cells were maintained in DMEM (25 m*M* glucose) supplemented with 10% foetal bovine serum, 2 m*M* GlutaMAX I and non-essential amino acids and were transfected using Lipofectamine and Plus Reagent according to the manufacturer's protocols. Briefly, cells were seeded at 40–50% confluence onto glass coverslips in a 24-well plate for 24 h. The wells were washed in OptiMEM reduced serum medium containing 2 m*M* GlutaMAX I. A transfection mixture consisting of 0.25 µg DNA and 1 µl Plus Reagent in 50 µl OptiMEM (per well) was prepared and allowed to incubate for 5 min at room temperature before combining with 1 µl Lipofectamine. The mixture was incubated for 25 min at room temperature to allow lipid-complex formation before being added to the prepared cells. The medium was replaced with complete culture medium after 3 h and the cells were fixed after 18–21 h.

2.9. Immunofluorescence microscopy

Cells were fixed and processed for immunofluorescence microscopy as described previously (Richards *et al.*, 2002) with the following exceptions: fixation in 4% paraformaldehyde was followed by permeabilization in 0.1% Triton X-100 in phosphate-buffered saline (PBS) (except when labelling with anti-Bcl-x_L, when a 5 min methanol treatment at 253 K was used) and the blocking solution was 0.5% bovine serum albumin in PBS. Experiments were viewed and imaged using either a Zeiss Axioplan 2 epifluorescent microscope or a Zeiss LSM 510 META confocal microscope.

2.10. Subcellular fractionation and Western blotting

HeLa cells transiently transfected with BinCARD-2 were fractionated as described previously (Whitehead *et al.*, 2001). Equal protein loads of the various fractions were analyzed by SDS–PAGE and Western blotting as described elsewhere (Richards *et al.*, 2006).

3. Results

3.1. BinCARD-CARD is monomeric

We screened several constructs of human BinCARD using a small-scale parallel processing approach that allowed us to rapidly identify which of these constructs could be produced in a soluble form (Puri *et al.*, 2006). Two constructs met these criteria: BinCARD-CARD (residues 3–101, corresponding to the CARD fold common to both human BinCARD isoforms) and BinCARD-2-Δ124–183 (equivalent to human BinCARD-2 residues 1–123 and lacking the transmembrane domain and C-terminal residues).

CARD proteins are thought to self-associate (Shiozaki *et al.*, 2002; Park *et al.*, 2007; Scott *et al.*, 2009), so we first tested whether either of these constructs could homo-oligomerize in solution. However, both proteins eluted as a single peak on

size-exclusion chromatography at a volume consistent with a monomer (Supplementary Fig. S2A). The oligomeric state of BinCARD-2-Δ124–183 was further evaluated using MALLS. At 5 mg ml^{-1}, the elution peak of BinCARD-2-Δ124–183 gave an average molecular weight of 13.8 kDa (Supplementary Fig. S2B), confirming that it is a monomer in solution (theoretical molecular mass of 14.4 kDa). These results suggest that neither BinCARD-CARD nor the soluble form of BinCARD-2 can self-associate on their own under the experimental conditions used.

3.2. Crystal structure of human BinCARD-CARD solved using a double-methionine mutant

Crystals of the BinCARD-CARD construct (triclinic symmetry, space group *P*1) grew from PEG-containing conditions and diffracted to high resolution. Assuming a solvent content of 34%, two molecules are predicted in the asymmetric unit. We unsuccessfully attempted to solve the structure by molecular replacement using low-sequence-identity templates from other CARD structures (13–22% identity to BinCARD-CARD). We then investigated multi-wavelength anomalous diffraction (MAD) phasing using selenomethionine. Because BinCARD-CARD has no native methionines, we engineered first one (L66M) and then two (F16M/L66M) methionines into the sequence to produce F16M/L66M BinCARD-CARD. These two residues were selected on the basis of their high degree of conservation as hydrophobic residues (including Met) in other Bcl10-interacting proteins. The single-mutation L66M SeMet protein crystals did not provide sufficient phasing power to solve the structure, but the double-mutant F16M/L66M SeMet protein crystals did generate a solution.

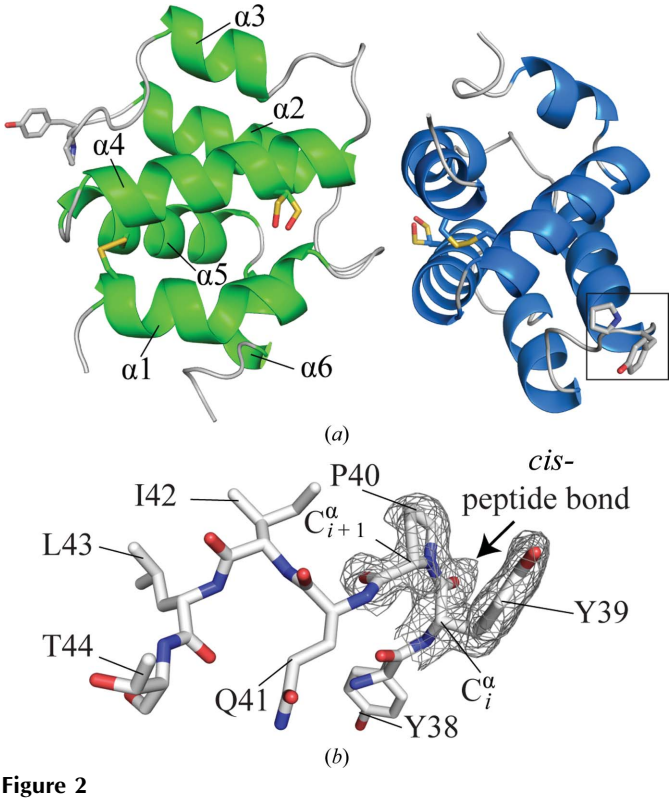

Figure 2
Crystal structure of BinCARD-CARD. (*a*) Cartoon representation of the BinCARD-CARD crystal structure showing the two molecules (green and blue) in the asymmetric unit, each comprising a canonical CARD fold of six α-helices. Side chains are shown in stick format for the three cysteines and the YP *cis*-peptide. (*b*) The boxed *cis*-peptide in (*a*) is enlarged to show the *cis*-peptide bond formed between residues Tyr39 and Pro40 from the YYPQILT loop linking helices 2 and 3 in more detail. The electron density shown corresponds to that from a $2F_o - F_c$ map contoured at 1σ.

The F16M/L66M SeMet protein crystals were isomorphous to the native crystals. However, the quality of the X-ray diffraction from the F16M/L66M SeMet crystals was highly variable and successful phasing by MAD required the use of a microfocus synchrotron beamline. This approach allowed screening of different regions of the crystal to find optimal points for measuring high-redundancy two-wavelength data from a single F16M/L66M SeMet crystal. The combination of the low-symmetry space group and the necessity for high-redundancy data for MAD phasing required the measurement of 1080° of data at both wavelengths. Using these data, the crystal structures of SeMet F16M/L66M BinCARD-CARD and native BinCARD-CARD were solved at resolutions of 1.40 and 1.57 Å, respectively (Table 1). Both the native and F16M/L66M SeMet structures of human BinCARD-CARD revealed two monomers in the asymmetric unit, with each monomer comprising an antiparallel six-α-helix bundle (Fig. 2*a*).

3.3. BinCARD-CARD structures incorporate a *cis*-proline

The crystal structures of both the native and the double-methionine mutant of BinCARD-CARD reveal that the protein incorporates a *cis*-peptide bond between residues Tyr39 and Pro40 in the loop connecting helices 2 and 3 (Fig. 2). Aromatic residues, especially tryptophan and tyrosine, are often found adjacent to prolines because they stabilize the *cis* conformation through aromatic and hydrophobic interactions (Zondlo, 2012). Moreover, *cis*-prolines are often associated with protein interactions (reviewed in Kay *et al.*, 2000) and can undergo *cis–trans* isomerization to act as a timer or switch to regulate activity (Lu *et al.*, 2007; Schwartz *et al.*, 2006).

We analyzed other structurally characterized CARD proteins to identify whether *cis*-prolines were a common feature of this group of proteins. However, we found no other instance of a *cis*-peptide bond. A structure-based sequence alignment of the structurally characterized CARDs (Fig. 3) suggests that the two residues forming the *cis*-peptide in BinCARD, Tyr39 and Pro40, correspond to an insertion in the α2–α3 loop of BinCARD relative to other CARDs. This indicates that if the *cis*-proline is important for function then this function is likely to be specific to BinCARD rather than to CARD proteins more generally.

3.4. The human BinCARD-CARD crystal structure reveals that all three cysteine residues are oxidized

An unexpected finding from the structure determination was that all three of the cysteine residues of native BinCARD-

CARD were oxidized in both monomers of the asymmetric unit. Thus, an intramolecular disulfide bond (right-hand hook conformation) was formed between Cys7 and Cys77, linking helices 1 and 5 (Fig. 4*a*) in both monomers. Also, additional density at Cys63 in both molecules of the native structure indicated oxidation, which was modelled as a cysteine sulfenic acid (CSO; Fig. 4*b*). A recent analysis of protein structures incorporating cysteines oxidized to CSO found an increased propensity for nearby Thr or other polar residues (Salsbury *et al.*, 2008). These are thought to lower the pK_a of the cysteine, making it more susceptible to modification. There is a similar preponderance of Thr residues near Cys63 of BinCARD in that Thr18 is 4 Å from the Cys63 sulfur and Thr14 and Ser67 are both within 8 Å (Fig. 4*c*).

In comparison to the native BinCARD-CARD structure, the refined F16M/L66M SeMet BinCARD-CARD crystal structure reveals partial oxidation: the disulfide of Cys7 and Cys77 was modelled as a mixture of both oxidized and reduced forms. Disulfide reduction in this SeMet-labelled crystal structure is likely to be a consequence of the long exposure to synchrotron radiation on the insertion-device beamline which was required to measure the high-redundancy data for MAD phasing. Radiation-induced reduction of disulfide bonds is often observed even in cryocooled crystals when intense third-generation synchrotron source radiation is used to measure diffraction data (Garman & Owen, 2006). There was no evidence for the oxidation of Cys63 to CSO in the SeMet-labelled crystal form.

We investigated the conditions used to generate the BinCARD-CARD crystals to identify factors that might contribute to cysteine oxidation. During purification, freshly prepared 2 m*M* DTT reducing agent was included in the dialysis and gel-filtration buffers. This addition would be expected to maintain the BinCARD-CARD cysteines in the reduced form. However, for crystallization of native BinCARD-CARD, a 1:1 ratio of 1 m*M* reduced and 1 m*M* oxidized L-glutathione was included. This ratio should also be reducing, but if the glutathione is stored at 277 K or room temperature for any length of time, the glutathione can convert to the oxidized form (Anderson, 1985). Because the glutathione was prepared a few days in advance, it is possible that cysteine oxidation of the native form may have occurred during crystallization as a consequence of using this additive. On the other hand, the F16M/L66M SeMet BinCARD-CARD protein was crystallized without using a glutathione additive and retains a disulfide bond (partially reduced by radiation damage) between Cys7 and Cys77. This indicates that the Cys7–Cys77 disulfide bond may form through air

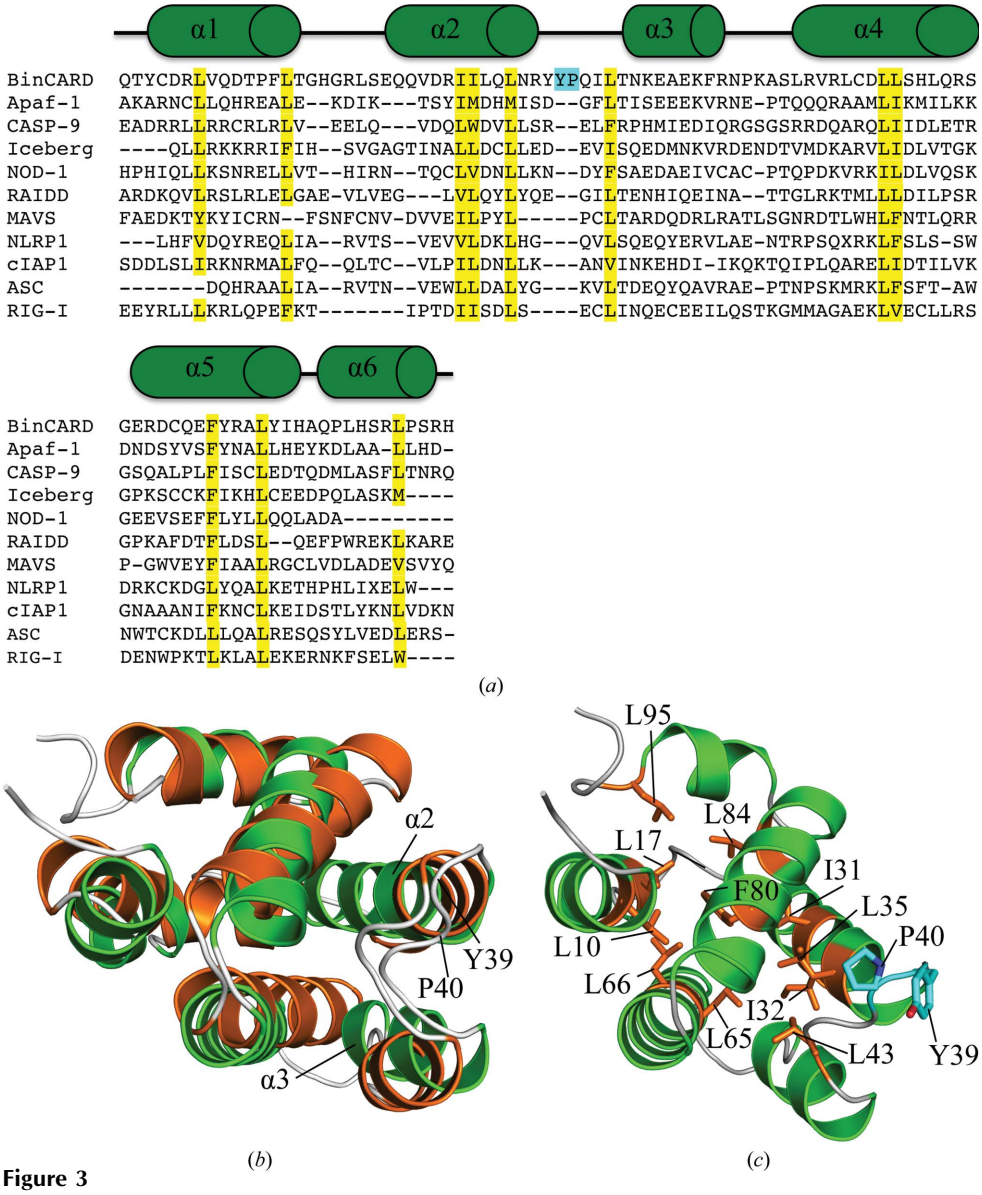

Figure 3
Comparison of CARDs of known structure. (*a*) Structure-based alignment prepared using the *DALI* server (Holm & Rosenström, 2010); secondary-structure elements of the BinCARD-CARD structure are shown above the sequences. Highly conserved hydrophobic residues are highlighted in yellow. Residues Tyr39 and Pro40 of the *cis*-peptide bond are highlighted in blue. (*b*) Superposition of BinCARD-CARD (green) and Apaf-1 CARD (PDB entry 1cy5; Vaughn *et al.*, 1999; orange) showing the relative arrangement of the six helices in both CARD structures. (*c*) Cartoon representation of BinCARD-CARD showing the 11 highly conserved core hydrophobic residues in orange and the YP residues of the *cis*-proline in blue.

Table 2
Superposition of BinCARD-CARD and other CARD structures.

	Resolution (Å) or NMR	PDB code	R.m.s.d.† (Å)	*Z*-score† (Å)	Sequence identity (%)	No. of aligned residues‡	Reference
NLRP1	3.1	3kat	1.8	11.3	19	81	—
ICEBERG	NMR	1dgn	1.9	11.9	13	84	Humke *et al.* (2000)
NOD1	2.0	2nsn	2.1	12.0	15	80	Coussens *et al.* (2007)
Apaf-1	1.3	1cy5	2.3	10.9	22	86	Vaughn *et al.* (1999)
RIG-I	NMR	2lwd	2.5	7.2	21	81	Ferrage *et al.* (2012)
cIAP1	NMR	2l9m	2.6	9.0	17	86	Lopez *et al.* (2011)
Procaspase-9	2.5	3ygs	2.9	10.4	20	89	Qin *et al.* (1999)
MAVS	2.1	2vgq	2.9	9.0	18	87	Potter *et al.* (2008)
RAIDD	NMR	3crd	2.9	8.4	20	87	Chou *et al.* (1998)
ASC	NMR	2kn6	3.2	7.0	18	79	de Alba (2009)

† R.m.s.d. and *Z*-score were calculated using the *DALI* server (Holm & Rosenström, 2010). ‡ The total number of residues in the BinCARD-CARD structure is 96.

oxidation over the 5 d that it takes crystals to grow. Together, these observations suggest that the oxidation of Cys7 and Cys77 occurs relatively easily, whereas the oxidation of Cys63 to CSO requires a more highly oxidizing environment.

The structural data from these two crystal structures of BinCARD-CARD, one with all three cysteines oxidized and the other with partial oxidation of the disulfide bond, allow analysis of the effect of cysteine oxidation on the protein structure. The region around Cys7 and Cys77 appears to be relatively unaffected by disulfide formation because the SeMet-labelled crystal structure shows no major conformational changes around these two residues. The only apparent difference is that Cys7 becomes more accessible in the reduced form. On the other hand, comparison of the native and SeMet-labelled crystal structures reveals that oxidation of Cys63 to CSO does induce a conformational change. In both molecules in the asymmetric unit, the side chain of Arg59 moves away from the side chain of Cys63 in oxidized BinCARD compared with the reduced structure. The C^{ζ} atom of Arg59 moves by 4 Å during this conformational change (Fig. 4*c*). The introduced selenomethionine residues in the SeMet structure showed no evidence of oxidation.

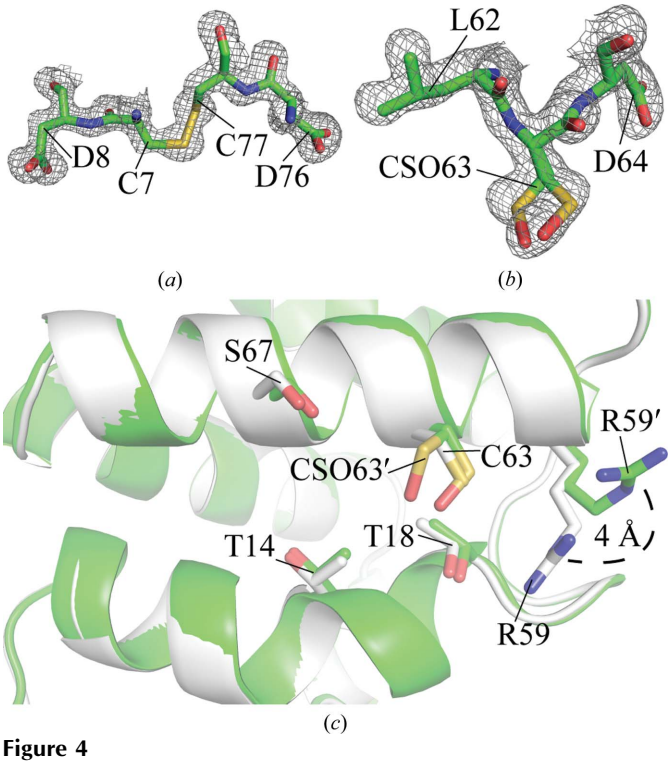

Figure 4
Comparison of oxidized and reduced Cys63. (*a*) Cys7 and Cys77 form a disulfide bond in the native structure. (*b*) Cys63 in the native structure was modelled as a cysteine sulfenic acid (CSO) in the two molecules of the asymmetric unit in the native structure. The electron density shown in (*a*) and (*b*) corresponds to that from a $2F_o - F_c$ map contoured at 1σ. (*c*) Cys63 is oxidized in the native structure (CSO63′, modelled in two alternate conformations; green) and not oxidized in the SeMet-labelled structure (Cys63; white). This change in oxidation state results in movement of the Arg59 side chain by 4 Å (R59′ in green for the native structure; R59 for the SeMet-labelled structure).

3.5. Comparison of BinCARD-CARD with other CARD structures

BinCARD-CARD shares 13–22% sequence identity with CARDs that have been structurally characterized (Table 2). The crystal structure of NOD1 CARD is the only other reported CARD-containing protein with oxidized cysteines. However, the disulfide bond in NOD1 CARD is unlike that in BinCARD-CARD. In NOD1 CARD, the two Cys39 residues from symmetry-related monomers form a disulfide bond that stabilizes a domain-swapped dimer structure (Srimathi *et al.*, 2008).

The structural homologues of BinCARD with the lowest root-mean-square deviations (r.m.s.d.s) are NLRP1 (PDB entry 3kat; Northeast Structural Genomics Consortium, unpublished work) and ICEBERG (PDB entry 1dgn; Humke *et al.*, 2000), with r.m.s.d.s of 1.8 Å for 81 C^{α} atoms and 1.9 Å for 84 C^{α} atoms, respectively (Table 2). Despite overall low sequence identity (19% to NLRP1 and 13% to ICEBERG), structure-based sequence alignment revealed 11 highly conserved hydrophobic residues across these proteins (Fig. 3). All except Leu43 are located in helical rather than loop regions and form a hydrophobic core (Fig. 3). This suggests that these residues are conserved to preserve the stability of the core CARD fold.

The lack of conserved residues on the surface of CARD indicates that CARD-family members may have evolved different interaction surfaces. Previous work showed that mutation of Leu65 of BinCARD-1 to alanine abolished its ability to bind to Bcl10 (Woo *et al.*, 2004). Leu65 is one of the 11 highly conserved hydrophobic core residues, suggesting that its role may be in maintaining the CARD fold rather than in mediating interaction with Bcl10.

BinCARD-1 and Bcl10 are thought to interact through their CARDs, so we investigated possible CARD–CARD inter-

faces of BinCARD using the crystal structure as a guide. One classic CARD–CARD interaction is defined by the Apaf-1–procaspase-9 complex (Qin *et al.*, 1999; Figs. 5*a* and 5*b*). The formation of this complex is mediated by charged surfaces on procaspase-9 and Apaf-1 and reinforced by van der Waals and hydrogen-bond interactions. Several residues on helices 1 and 4 of procaspase-9 form a basic patch that is complementary to an acidic patch on Apaf-1 formed from residues located in helices 2 and 3 (Qin *et al.*, 1999).

There are only three basic residues on the helix 1–4 surface of BinCARD (Arg59, Arg61 and Arg71) and these do not form a contiguous basic surface (Fig. 5*c*). However, there are three acidic residues on the helix 2–3 surface of BinCARD (Glu25, Asp29 and Glu49) that form an acidic patch on the surface of BinCARD-CARD (Fig. 5*d*). Interestingly, BinCARD-CARD residues contributing to a region adjacent to but not including the acidic patch are highly conserved across all species (Fig. 5*f*), whereas residues contributing to the reverse surface appear to be poorly conserved in comparison (Fig. 5*e*). Overall, this suggests the possibility that the helix 2–3 surface of BinCARD-CARD (Fig. 5*f*) may interact with a complementary surface on Bcl10.

3.6. BinCARD isoforms 1 and 2 exhibit different subcellular localization

BinCARD-1 has previously been shown to localize to nuclei when expressed in HeLa cells and to redistribute into the cytosol upon co-expression with Bcl10 (Woo *et al.*, 2004). BinCARD-2, the dominantly expressed isoform in immune cells, has a predicted transmembrane helix C-terminal to the CARD, indicating that it is a membrane protein. Sequence analysis did not reveal any conserved membrane-localization sequences (*e.g.* signal peptide or mitochondrial targeting sequence), as has also been observed for other tail-anchored proteins (Rapaport, 2003). Therefore, while we expected BinCARD-2 to have a different distribution to the cytoplasmic/nuclear distribution of BinCARD-1, it was not possible to predict which membrane it would target.

To examine the subcellular localization of human BinCARD-2 in comparison to BinCARD-1 and to the CARD region only (residues 1–100, designated BinCARD-N; Supplementary Fig. S1B), we transiently expressed C-terminal V5/His-tagged versions of the proteins in HeLa cells. Immunofluorescence microscopy revealed that BinCARD-N was both cytoplasmic and nuclear, and we confirmed the results of Woo *et al.* (2004) showing that BinCARD-1 was predominantly nuclear (Supplementary Fig. S1C). However, the distribution pattern for BinCARD-2 was distinct from these two and suggested localization to the endoplasmic reticulum (ER) and mitochondria (Supplementary Fig. S1B, top panel).

Coexpression of BinCARD-2 with a well characterized ER marker, isoprenylcysteine carboxyl methyltransferase (ICMT; Dai *et al.*, 1998), resulted in extensive colocalization of the two proteins, confirming ER localization of isoform 2 (Supplementary Fig. S1C, middle panel). However, co-labelling of BinCARD-2 transfected cells for the outer mitochondrial membrane marker Bcl-x_L also revealed partial colocalization (Supplementary Fig. S1C, bottom panel). Furthermore,

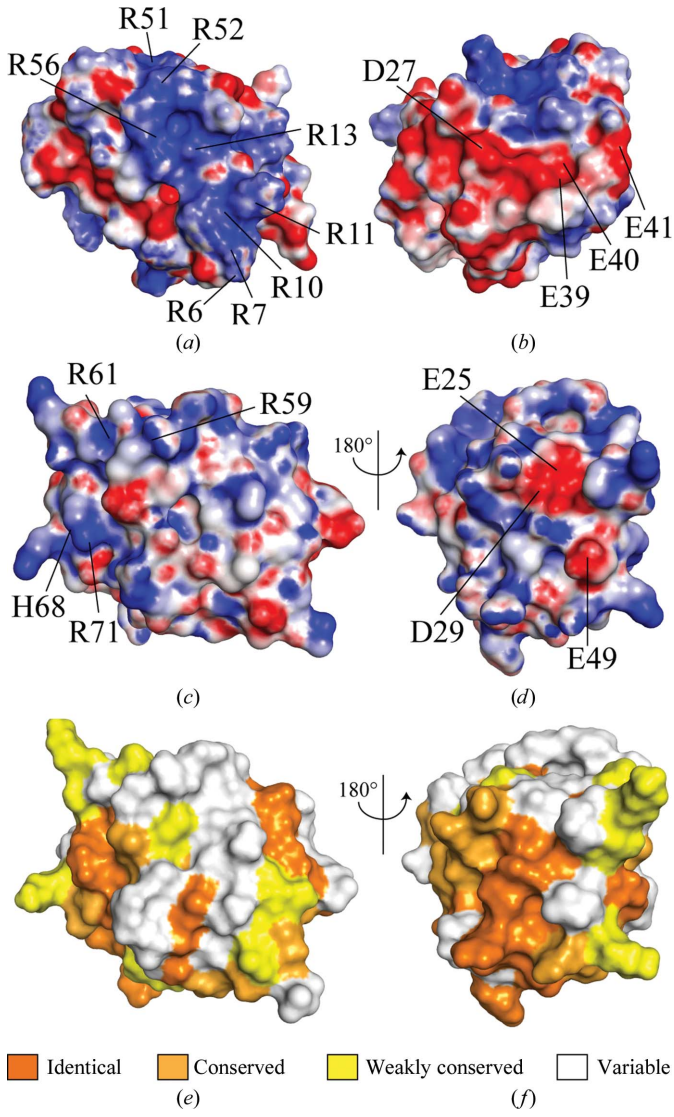

Figure 5
Electrostatic surface features of CARD proteins. (*a*) Procaspase-9 CARD (PDB entry 3ygs; Qin *et al.*, 1999) has an extensive positively charged surface contributed by helices 1 and 4. (*b*) Apaf-1 CARD (PDB entry 3ygs; Qin *et al.*, 1999) has an extensive negatively charged surface contributed by helices 2 and 3 on the reverse surface. (*c*) The equivalent helices 1 and 4 of BinCARD-CARD do not generate a distinct positively charged surface. (*d*) The electrostatic potential surface contributed by helices 2 and 3 of BinCARD-CARD has a more limited acidic patch than that of Apaf-1 CARD. All three structures were superimposed, so that (*a*) and (*c*) represent equivalent surfaces of procaspase-9 and BinCARD-CARD and (*b*) and (*d*) represent equivalent surfaces of Apaf-1 and BinCARD-CARD. The electrostatic potential mapped onto the surface was calculated using *APBS* (Baker *et al.*, 2001) and displayed in *PyMOL*. The electrostatic potential is shown over the range $-10kT$/e (negatively charged) to $+10kT$/e (positively charged). (*e*, *f*) Sequence conservation is shown mapped onto the surfaces of (*e*) helices 1 and 3 and (*f*) helices 2 and 3 of BinCARD-CARD shown in the same orientation as in (*c*) and (*d*), respectively. Sequence conservation was based on a *T-Coffee* multiple sequence alignment (Notredame *et al.*, 2000; Supplementary Fig. S3). The surface is coloured orange, light orange, yellow and white to show residues that are identical, conserved, weakly conserved or variable, respectively, across BinCARD-CARD sequences.

subcellular fractionation of lysates revealed enrichment of BinCARD-2 in a Bcl-x_L-enriched mitochondrial fraction. In addition to full-length BinCARD-2, the antibody to the C-terminal V5 tag also detected an N-terminally truncated form in this fraction indicative of proteolytic cleavage (Supplementary Fig. S1D). Collectively, these data demonstrate that BinCARD-2 is dually targeted to the ER and mitochondria.

4. Discussion

The crystal structure of native BinCARD-CARD revealed that all three cysteines of the CARD were oxidized. Cys7 and Cys77 form a disulfide bond in the native structure which is partially reduced in the SeMet-labelled crystal structure, allowing differences between the reduced and oxidized forms to be assessed. Cys63 was also oxidized and we modelled this as multiple conformations of cysteine sulfenic acid. If cysteine oxidation is important for function, we would expect to observe conservation of the cysteines in BinCARD proteins from other organisms. Indeed, analysis of BinCARD sequences from several organisms indicates that Cys63 is conserved in most mammals, but not in birds, reptiles or fish. Moreover, the cysteines Cys7 and Cys77 that form the disulfide are conserved in all of the BinCARDs aligned in Supplementary Fig. S3, except for that from a fish (atlantic salmon).

We also identified a *cis*-peptide bond between Tyr39 and Pro40 in a loop comprising the sequence YYPQIL. The tyrosine in this sequence may be important for stabilizing the *cis*-proline conformation. Again, if the *cis*-proline is important for function the loop sequence would be expected to be highly conserved. The sequence alignment of BinCARD-CARDs shows that the six-residue loop is identical except for the first of the two tyrosines (Supplementary Fig. S3).

Although CARDs have a common fold, their sequence identity is low, suggesting that their electrostatic surfaces, including interacting regions, vary. CARDs often have an asymmetric charge distribution that contributes to electrostatically driven CARD–CARD interactions: for example, a large basic patch on procaspase-9 interacts with a large acidic patch on Apaf-1 to form the CARD–CARD interaction (Qin *et al.*, 1999; Figs. 5*a* and 5*b*). The electrostatic surface of BinCARD-CARD does not present a basic surface like that of procaspase-9, although a small acidic patch is present on the equivalent surface to that found on Apaf-1. The residues forming the acidic region in BinCARD are Glu25, Asp29 and Glu49: Glu25 is conserved across all of the sequences analyzed in Supplementary Fig. S3 except for that from atlantic salmon, which instead has a threonine with an acidic residue on either side; Asp29 is conserved in all of the sequences and Glu49 is acidic in all but two of the sequences. This suggests the possibility that the acidic patch present on the surface of human BinCARD-CARD may be conserved in almost all other BinCARDs. However, a region adjacent to the acidic patch of human BinCARD-CARD is even more highly conserved (Fig. 5*f*), suggesting that this surface may contribute the interaction interface for Bcl-10.

Many CARD-containing proteins are susceptible to cysteine oxidation, including caspase-1 and caspase-9. For example, the oxidation of redox-sensitive cysteines inhibits caspase-1-mediated inflammatory processes (Meissner *et al.*, 2008). Cysteine oxidation of caspase-9 by mitochondrial reactive oxygen species (ROS) is important for caspase-9 activation because it stabilizes the interaction between caspase-9 and Apaf (Zuo *et al.*, 2009). However, no structural information is available for the effect of cysteine oxidation on these CARD proteins. Whilst we cannot rule out the possibility that the cysteine oxidation observed in the BinCARD crystal structures is an artefact of protein isolation, purification or crystallization, the conservation of the three cysteines supports the notion that they may play an important role, perhaps in redox regulation or sensing.

We showed that the two isoforms of human BinCARD are differentially expressed in all immune-cell populations examined, with BinCARD-2 being the more highly expressed isoform. The BinCARD-1 splice isoform predominantly localizes to the nucleus, whereas BinCARD-2, the splice isoform with a C-terminal transmembrane domain, is dually targeted to the ER and mitochondria. Other proteins that are dually localized to the ER and the outer membrane of mitochondria include several members of the Bcl-2 family of apoptosis regulators (*e.g.* Bcl-2, BAX and BAK). The Bcl-2 family consists of both pro-apoptotic and anti-apoptotic regulators that have important functions at the ER and mitochondria during responses to cellular stress such as the unfolded protein response (UPR), autophagy and calcium release from the ER (Rolland & Conradt, 2010).

Many of the characteristics of BinCARD-2 are reminiscent of another CARD protein, MAVS (also known as IPS-1, VISA or Cardif), that like BinCARD-2 has an N-terminal CARD and a C-terminal transmembrane domain. MAVS is also localized to the mitochondrial outer membrane and is a critical mediator of the viral RNA-sensing signalling pathways, which result in downstream NFκB activation (Hiscott *et al.*, 2006). MAVS is activated by CARD–CARD interactions with the viral RNA-sensing protein RIG-I. This results in homo-oligomerization of MAVS *via* its CARD to form large filaments that are capable of activating downstream signalling. Similarly to Bcl10, MAVS activation and signalling are dependent on oligomerization of its CARD (Hou *et al.*, 2011). A cleaved form of MAVS lacking the N-terminal CARD was also detected in mitochondrial membranes (similar to our finding for BinCARD-2), but this form failed to be incorporated into MAVS oligomers. Removal of the transmembrane domain of MAVS prevents its mitochondrial localization (Li *et al.*, 2005), as we also found for BinCARD-2. This modification also prevents the induction of downstream signalling by MAVS, highlighting the importance of the mitochondrial localization for activity (Li *et al.*, 2005).

Mitochondrial redox processes are an attractive possibility for BinCARD-2 function, because such processes underpin apoptosis, *inter alia*, a highly regulated process already asso-

ciated with CARD–CARD interactions (Zhou *et al.*, 1999; Seth *et al.*, 2005). Indeed, there are further curious parallels with MAVS, including the activation of MAVS by mitochondrial ROS to trigger innate immune signalling (Arnoult *et al.*, 2009).

We speculate that the three modifiable cysteines of BinCARD-2 could enable it to act as a tunable redox sensor, whereby the presence of reactive oxygen species might first induce disulfide formation between Cys7 and Cys77 and then progressively oxidize Cys63 to a cysteine sulfenic acid.

We thank Jasmyn Dunn and Greg Kelly for providing reagents, Felicia Goh and Juliana Ariffin for technical assistance and Rob Parton, David Drew and Gunnar von Heijne for helpful discussions. We thank Glenn King for MALLS access. We acknowledge use of the University of Queensland Remote Operation Crystallization and X-ray Diffraction Facility and the assistance of Karl Byriel and Gordon King. X-ray data were collected on the MX2 microfocus beamline at the Australian Synchrotron, Australia. MJS and JLM are members of the Australian Infectious Diseases Research Centre of the University of Queensland. This project was funded by Australian Research Council (ARC) grant DP0770465 to JLM, BK and SK. JLM is an ARC Australian Laureate Fellow (FL0992138) and Honorary National Health and Medical Research Council (NHMRC) Research Fellow (455829), BK is an NHMRC Research Fellow (APP1003325), MJS is an ARC Future Fellow (FT100100657) and Honorary NHMRC Research Fellow (APP1003470) and JMH was supported by an NHMRC RD Wright Fellowship (APP401748).

References

Adams, P. D. *et al.* (2010). *Acta Cryst.* D**66**, 213–221.
Alba, E. de (2009). *J. Biol. Chem.* **284**, 32932–32941.
Anderson, M. E. (1985). *Methods Enzymol.* **113**, 548–555.
Arnoult, D., Soares, F., Tattoli, I., Castanier, C., Philpott, D. J. & Girardin, S. E. (2009). *J. Cell Sci.* **122**, 3161–3168.
Baker, N. A., Sept, D., Joseph, S., Holst, M. J. & McCammon, J. A. (2001). *Proc. Natl Acad. Sci. USA*, **98**, 10037–10041.
Chen, V. B., Arendall, W. B., Headd, J. J., Keedy, D. A., Immormino, R. M., Kapral, G. J., Murray, L. W., Richardson, J. S. & Richardson, D. C. (2010). *Acta Cryst.* D**66**, 12–21.
Chou, J. J., Matsuo, H., Duan, H. & Wagner, G. (1998). *Cell*, **94**, 171–180.
Combet, C., Blanchet, C., Geourjon, C. & Deléage, G. (2000). *Trends Biochem. Sci.* **25**, 147–150.
Coussens, N. P., Mowers, J. C., McDonald, C., Nuñez, G. & Ramaswamy, S. (2007). *Biochem. Biophys. Res. Commun.* **353**, 1–5.
Dai, Q., Choy, E., Chiu, V., Romano, J., Slivka, S. R., Steitz, S. A., Michaelis, S. & Philips, M. R. (1998). *J. Biol. Chem.* **273**, 15030–15034.
Edeling, M. A., Guddat, L. W., Fabianek, R. A., Halliday, J. A., Jones, A., Thöny-Meyer, L. & Martin, J. L. (2001). *Acta Cryst.* D**57**, 1293–1295.
Emsley, P. & Cowtan, K. (2004). *Acta Cryst.* D**60**, 2126–2132.
Ferrage, F., Dutta, K., Nistal-Villán, E., Patel, J. R., Sánchez-Aparicio, M. T., De Ioannes, P., Buku, A., Aseguinolaza, G. G., García-Sastre, A. & Aggarwal, A. K. (2012). *Structure*, **20**, 2048–2061.
Garman, E. F. & Owen, R. L. (2006). *Acta Cryst.* D**62**, 32–47.
Hiscott, J., Lin, R., Nakhaei, P. & Paz, S. (2006). *Trends Mol. Med.* **12**, 53–56.
Holm, L. & Rosenström, P. (2010). *Nucleic Acids Res.* **38**, W545–W549.
Hou, F., Sun, L., Zheng, H., Skaug, B., Jiang, Q.-X. & Chen, Z. J. (2011). *Cell*, **146**, 448–461.
Humke, E. W., Shriver, S. K., Starovasnik, M. A., Fairbrother, W. J. & Dixit, V. M. (2000). *Cell*, **103**, 99–111.
Kabsch, W. (2010). *Acta Cryst.* D**66**, 125–132.
Kay, B. K., Williamson, M. P. & Sudol, M. (2000). *FASEB J.* **14**, 231–241.
Kersse, K., Verspurten, J., Vanden Berghe, T. & Vandenabeele, P. (2011). *Trends Biochem. Sci.* **36**, 541–552.
Li, X.-D., Sun, L., Seth, R. B., Pineda, G. & Chen, Z. J. (2005). *Proc. Natl Acad. Sci. USA*, **102**, 17717–17722.
Lopez, J., John, S. W., Tenev, T., Rautureau, G. J., Hinds, M. G., Francalanci, F., Wilson, R., Broemer, M., Santoro, M. M., Day, C. L. & Meier, P. (2011). *Mol. Cell*, **42**, 569–583.
Lu, K. P., Finn, G., Lee, T. H. & Nicholson, L. K. (2007). *Nature Chem. Biol.* **3**, 619–629.
McPhillips, T. M., McPhillips, S. E., Chiu, H.-J., Cohen, A. E., Deacon, A. M., Ellis, P. J., Garman, E., Gonzalez, A., Sauter, N. K., Phizackerley, R. P., Soltis, S. M. & Kuhn, P. (2002). *J. Synchrotron Rad.* **9**, 401–406.
Meissner, F., Molawi, K. & Zychlinsky, A. (2008). *Nature Immunol.* **9**, 866–872.
Notredame, C., Higgins, D. G. & Heringa, J. (2000). *J. Mol. Biol.* **302**, 205–217.
Park, H. H., Logette, E., Raunser, S., Cuenin, S., Walz, T., Tschopp, J. & Wu, H. (2007). *Cell*, **128**, 533–546.
Potter, J. A., Randall, R. E. & Taylor, G. L. (2008). *BMC Struct. Biol.* **8**, 11.
Pruitt, K. D., Tatusova, T., Klimke, W. & Maglott, D. R. (2009). *Nucleic Acids Res.* **37**, D32–D36.
Puri, M., Robin, G., Cowieson, N., Forwood, J. K., Listwan, P., Hu, S.-H., Guncar, G., Huber, T., Kellie, S., Hume, D. A., Kobe, B. & Martin, J. L. (2006). *Biomol. Eng.* **23**, 281–289.
Qin, H., Srinivasula, S. M., Wu, G., Fernandes-Alnemri, T., Alnemri, E. S. & Shi, Y. (1999). *Nature (London)*, **399**, 549–557.
Rapaport, D. (2003). *EMBO Rep.* **4**, 948–952.
Richards, A. A., Stang, E., Pepperkok, R. & Parton, R. G. (2002). *Mol. Biol. Cell*, **13**, 1750–1764.
Richards, A. A., Stephens, T., Charlton, H. K., Jones, A., Macdonald, G. A., Prins, J. B. & Whitehead, J. P. (2006). *Mol. Endocrinol.* **20**, 1673–1687.
Rolland, S. G. & Conradt, B. (2010). *Curr. Opin. Cell Biol.* **22**, 852–858.
Ruland, J., Duncan, G. S., Elia, A., del Barco Barrantes, I., Nguyen, L., Plyte, S., Millar, D. G., Bouchard, D., Wakeham, A., Ohashi, P. S. & Mak, T. W. (2001). *Cell*, **104**, 33–42.
Salsbury, F. R., Knutson, S. T., Poole, L. B. & Fetrow, J. S. (2008). *Protein Sci.* **17**, 299–312.
Schroder, K. *et al.* (2012). *Proc. Natl Acad. Sci. USA*, **109**, E944–E953.
Schwartz, T. U., Schmidt, D., Brohawn, S. G. & Blobel, G. (2006). *Proc. Natl Acad. Sci. USA*, **103**, 6823–6828.
Scott, F. L., Stec, B., Pop, C., Dobaczewska, M. K., Lee, J. J., Monosov, E., Robinson, H., Salvesen, G. S., Schwarzenbacher, R. & Riedl, S. J. (2009). *Nature (London)*, **457**, 1019–1022.
Seth, R. B., Sun, L., Ea, C.-K. & Chen, Z. J. (2005). *Cell*, **122**, 669–682.
Sheldrick, G. M. (2010). *Acta Cryst.* D**66**, 479–485.
Shiozaki, E. N., Chai, J. & Shi, Y. (2002). *Proc. Natl Acad. Sci. USA*, **99**, 4197–4202.
Srimathi, T., Robbins, S. L., Dubas, R. L., Hasegawa, M., Inohara, N. & Park, Y. C. (2008). *Biochemistry*, **47**, 1319–1325.
Stols, L., Gu, M., Dieckman, L., Raffen, R., Collart, F. R. & Donnelly, M. I. (2002). *Protein Expr. Purif.* **25**, 8–15.
Studier, F. W. (2005). *Protein Expr. Purif.* **41**, 207–234.

Thome, M. & Tschopp, J. (2002). *Curr. Biol.* **12**, R45.
Vaughn, D. E., Rodriguez, J., Lazebnik, Y. & Joshua-Tor, L. (1999). *J. Mol. Biol.* **293**, 439–447.
Vonrhein, C., Blanc, E., Roversi, P. & Bricogne, G. (2007). *Methods Mol. Biol.* **364**, 215–230.
Whitehead, J. P., Molero, J. C., Clark, S., Martin, S., Meneilly, G. & James, D. E. (2001). *J. Biol. Chem.* **276**, 27816–27824.
Winn, M. D. *et al.* (2011). *Acta Cryst.* D**67**, 235–242.
Woo, H.-N., Hong, G.-S., Jun, J.-I., Cho, D.-H., Choi, H.-W., Lee, H.-J., Chung, C.-W., Kim, I.-K., Jo, D.-G., Pyo, J.-O., Bertin, J. & Jung, Y.-K. (2004). *FEBS Lett.* **578**, 239–244.
Zhou, P., Chou, J., Olea, R. S., Yuan, J. & Wagner, G. (1999). *Proc. Natl Acad. Sci. USA*, **96**, 11265–11270.
Zondlo, N. J. (2012). *Acc. Chem. Res.*, doi:10.1021/ar300087y.
Zuo, Y., Xiang, B., Yang, J., Sun, X., Wang, Y., Cang, H. & Yi, J. (2009). *Cell Res.* **19**, 449–457.